

# Dynamical Josephson Effects in Atomically-Thin NbSe<sub>2</sub>

S. Tran,<sup>1</sup> J. Sell,<sup>1</sup> and J. R. Williams<sup>1</sup>

<sup>1</sup>*Department of Physics, Joint Quantum Institute and the Center for Nanophysics and Advanced Materials, University of Maryland, College Park, MD 20742, USA*

(Dated: December 15, 2024)

The advent of atomically-thin materials has ushered new platforms for studying condensed-matter physics in two-dimensions. Recently, there has been a strong thrust towards isolating graphene-like material with interactions between the carriers making possible correlated states at low temperatures. One such material, NbSe<sub>2</sub> [1], has a well-studied past due to the interesting states arising from the competition with a co-existing charge-density wave [2, 3] and possible multi-band superconductivity [4–6]. More recently, NbSe<sub>2</sub> has been studied in its two dimensional form, where novel types of superconductivity (Ising) [7] and transition to Bragg glasses have been observed [8, 9]. Here an investigation of the superconducting to normal state transition is detailed, and it is found it is driven by a localized slip in the phase of the superconducting order parameter. These phase slips produce dynamically-created Josephson junctions, which enable the elucidation of two novel properties of the superconducting state in NbSe<sub>2</sub>. The first is a coupling of the Josephson current and the collective motion of the charge-density wave, resulting in a modification of the Shapiro step diagram observed under the application of microwave radiation. The second is a Josephson effect that possesses a modified shape and step height seen in its dependence on the applied RF radiation power. This effect – unlike any known Josephson behavior – exhibits an insensitivity to magnetic fields. We discuss possible origins of the latter effect, suggesting it lies in the multiband nature of superconductivity in NbSe<sub>2</sub> [10]. Each result expands the knowledge of the superconducting state of NbSe<sub>2</sub>, sheds light on the nature of materials in which superconductivity both competes with other collective phenomena and is multiband in nature. Further, this work opens new paradigms for electronics [11, 12] and quantum computation applications [13, 14] in transition metal dichalcogenides.

In this work we fabricate mesoscale devices formed from NbSe<sub>2</sub> thin films, focusing on the transition from the superconducting state to normal state as a function of applied DC current ( $I_{DC}$ ) and magnetic field  $B$  perpendicular to the surface of the NbSe<sub>2</sub>. In particular, magnetic fields or currents can drive the system out of

equilibrium and these effects can alter the behavior of the superconductor, even in simple measurements like the  $I - V$  characteristics. For example, shown in Fig. 1a is the measured differential resistance  $r = dV/dI$  versus  $I_{DC}$  for a NbSe<sub>2</sub> sample with a thickness of  $\sim 12$  nm. As is evident, the pattern is much more complex than a simple transition from a superconducting state to a normal one seen in bulk superconductors. This indicates that another mechanism may drive this transition and modify the transport in the normal state. Prominent in the measured  $r$  of Fig 1a is a semi-regular series of peaks. Upon application of  $B$ , the prominence of these peaks fades at  $B \sim 200$  mT. The magnitude of this field corresponds to the field at which a regular lattice of flux takes shape [15], suggesting that flux plays a role in the complex pattern seen in  $r$  at  $B = 0$ .

Dynamic incorporation of flux via the applied current is known to modify the transport in superconductors. In two-dimensional superconductors where the width of the film is larger than both the coherence length  $\xi$  and the penetration depth, flux can play an important role in the transition from a superconductor to a metallic conductor [16]. One type of transition is enabled by an applied current, whereby the superconducting order parameter slips by  $2\pi$ . In two dimensions this phase slip line (PSL) arises from kinematic chains of vortices which band to-

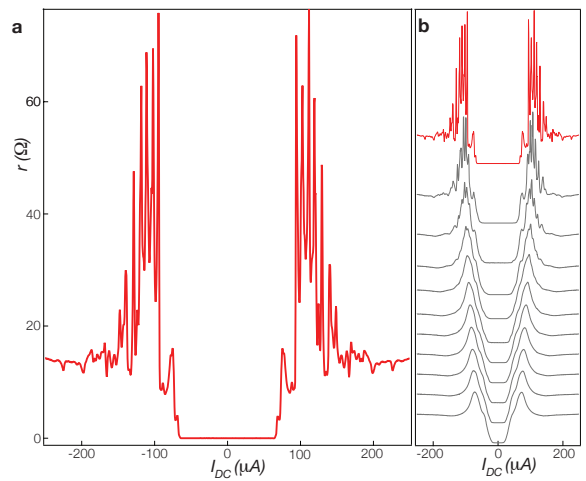


FIG. 1: **a.** Differential resistance  $r$  as a function of DC current  $I_{DC}$  taken at  $B = 0$  and  $T = 1.2$  K. Rather than a simple superconducting to normal state transition, a series of peaks in  $r$  are observed. **b.**  $r$  as a function of  $B$  taken between 0 and 1 T in 0.1 T steps. The peaks in  $r$  die off around  $B = 0.2$  T.

gether to produce a junction between two adjacent superconductors [17]. This forms a Josephson junction with a length of  $\sim \xi$ . The effects of PSLs on DC electrical transport have recently been observed in  $\text{NbSe}_2$  [18]. Here we demonstrate superconducting quantum interference across a PSL that creates a Josephson junction by addressing the junction with RF radiation. Should there be a junction created by a PSL, RF radiation mixed with the internal Josephson frequency should produce steps in the  $I - V$  curve (or peaks in  $r$ ), or Shapiro steps [19].

Fig 2a show  $r$  as a function of the  $I_{DC}$  and  $P$ , the power of the  $f = 3 \text{ GHz}$  RF radiation applied at the top of the cryostat (i.e. it does not include the attenuation incurred from the electrical path to the sample) for a sample of  $\sim 10 \text{ nm}$  in thickness. Plots of this type are referred to Shapiro step diagrams in this Letter. A regular pattern of peaks in  $r$  are observed. The area under the peaks in  $r$  (corresponding to the step height in a I-V curve) have a frequency dependence. As shown in Fig. 2b, the step height of the  $I - V$  curve obtained from integration of  $r$  produce steps heights of approximately  $2 \mu\text{V}/\text{GHz}$ , identifying the peaks as Shapiro steps arising from the junction formed by the kinematic vortices.

Two key features help to explain the deviations from a Shapiro step diagram common to conventional Josephson junctions. The first is that the Josephson coupling only turns on at a finite current associated with the formation of a PSL. The data of Fig. 2a allows for the identification of two PSLs corresponding to the transition from black to purple (at  $|I_{DC}|=500 \mu\text{A}$  at  $P = 0 \text{ dBm}$ ) and from purple to yellow (at  $|I_{DC}|=600 \mu\text{A}$  at the same power). It is only after these slips form that oscillations in  $r$  are observed. A broad white feature around  $|I_{DC}|=800 \mu\text{A}$  marks the transition to the normal state. One further feature, a dark depression of  $r$ , is distinct in the the data of Fig. 2a in that the power dependence follow a different trajectory than the power dependence of the PSLs and the transition to the normal state (this feature is indicated by a white arrow on the positive current side). This feature is not captured in the simulation of the Shapiro diagram using just PSLs.

In the normal state,  $\text{NbSe}_2$  undergoes a charge density wave transition at a temperature of  $33 \text{ K}$  in the bulk and a temperature that is layer-number dependent in thin films [20]. Motion of a sliding CDW is described by an equation that is very similar to Josephson junctions. For a Josephson junction weak-link comprised of a CDW material, coupling between the the Josephson current and the sliding motion of the CDW can affect the  $I - V$  curves when the length of the junction (the distance between the two superconducting leads) is of order a coherence length [21]. For  $\text{NbSe}_2$ , this coherence length is  $\sim 10 \text{ nm}$  [22], a length scale difficult to achieve by conventional lithographic techniques. However, here the junction length is automatically set to this length scale, making the results of Ref. [21] applicable to our junc-

tions. Simulations derived from the governing equations of a CDW weak link Josephson junction as:

$$I = I_C \sin \varphi + \frac{eN}{\pi} \dot{\chi} + \frac{\hbar}{2eR_N} \dot{\varphi} + I_{AC} \sin \Omega t, \quad (1)$$

$$\frac{\hbar \dot{\varphi}}{2e} = V_T \sin \chi + \frac{e}{\pi} NR_c \dot{\chi}, \quad (2)$$

where  $I_C$  and  $\varphi$  are from the conventional Josephson relations,  $I_{AC}$  and  $\Omega$  are the AC drive amplitude and frequency,  $V_T$  is the threshold voltage for CDW motion,  $R_c$  is the dissipation the CDW in motion,  $N$  is the number of 1D CDW chains, and  $\chi$  is the phase of the CDW (see the Supplementary Info [23] for more detail). Using the values of  $R_c=20$ ,  $V_T = 0.8$ ,  $N = 1$ ,  $I_C = R_N = 1$ ,  $\hbar = 1$ ,  $e = 1$ ,  $\Omega = 0.03$ , simulations show a dip in  $r$  between the second phase slip line and the transition to the normal state that has a power dependence distinct from the superconducting features of the diagram. Hence we correlate this dip with CDW existing in the normal region of the Josephson junction. To uncover the origin of this depression, we numerically integrate Eqs. 16a,b of Ref [21], finding that the origin is the mode-locking between the CDW and the Josephson current (i.e. between  $\varphi$  and  $\chi$ ) [23].

Moving to the study of two thinner samples (Sample I and II) of  $\sim 9 \text{ nm}$  and  $6 \text{ nm}$ , respectively, more structure is generated for a device subjected to DC currents

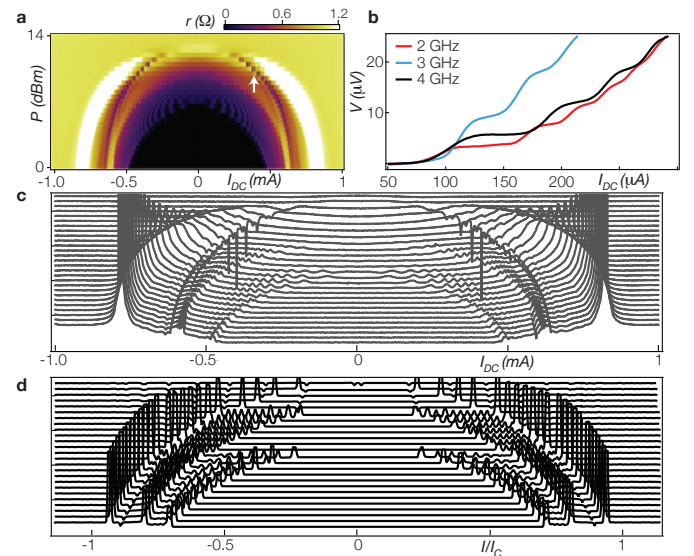


FIG. 2: **a.** Shapiro step diagram  $r(I_{DC}, P)$  taken at  $T=1.2 \text{ K}$ . At the appearance of the first PSL, oscillations in  $r$  are observed. In addition, a depression of  $r$  (indicated with a white arrow where it crosses the transition to the normal state) possess a  $P$  dependence different than the PSL. **b.** The frequency dependence of the step height increases with frequency with a magnitude of  $\sim h f / 2e$ . **c.** Slices of  $r$  from 2a. showing oscillations resulting from the applied RF radiation, matching well with simulations in **d.**

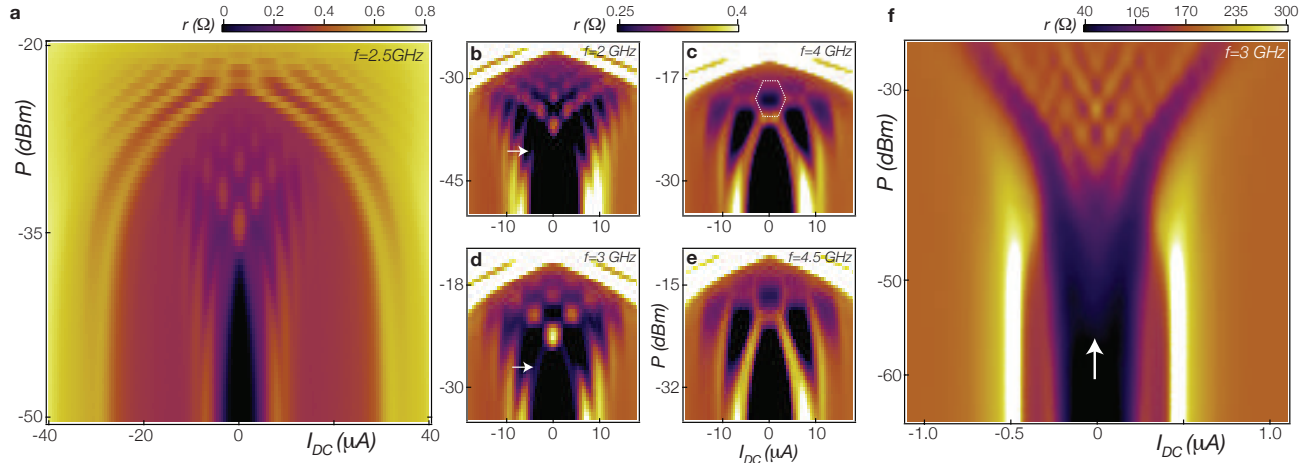


FIG. 3: **a.** Shapiro step diagram for Sample I showing “inner” and “outer” Josephson features. **b-e.** Frequency dependence of the inner features showing a Bessel-function-like dependence of the step features. Some unconventional features are observed: a step height which is not independent of power (white arrow) and hexagonal step width (white dashed line). All graphs in b-e have axes  $P$  vs.  $I_{DC}$ . **f.** Unlike the conventional Josephson effect where the steps originate from critical current, the step features begin at  $I_{DC} = 0$  (white arrow).

and RF radiation. Observed in Fig. 3a for Sample I are two distinct collections of oscillations of  $r$ . The first occurring at the transition identified as the formation of a PSL when the device is measured in the absence of RF radiation. This transition is visible in Fig. 3a at a value of  $|I_{DC}|=30 \mu\text{A}$  at  $P=-45\text{dBm}$ , following a power dependence similar to what was observed for the PSL in Fig. 2a. In addition, there are features that below this value of  $I_{DC}$ , i.e. before a PSL line can be identified in that absence of RF radiation. We refer to these features which become prevalent under RF radiation as the “inner” features and those associated with the PSL as the “outer” features.

To establish that these peaks in  $r$  originate from a Josephson-like relation, the frequency dependence of the peaks are shown in Fig. 3b-e. As the frequency increases, the peaks become more pronounced and the  $I_{DC}$  spacing between peaks increases. The pattern is reminiscent of the Bessel function dependence of the Shapiro step width that dictate the pattern observed in conventional Shapiro diagrams [19]. This power and frequency dependence of the shape of this pattern is set by a characteristic frequency  $f_c = 2eV_C/h = 2eI_C R_N/h$ . Hence, it is possible to extract the approximate strength of the superconducting order parameter associated with the Josephson-like phenomena without an explicit value for either  $I_C$  or  $R_N$  for the inner features. By matching the frequency dependence of the patterns, we are able to extract an  $I_C R_N$  product of  $14 \mu\text{V}$  for Sample I and  $44 \mu\text{V}$  for Sample II. For conventional Josephson junctions, this product is a proxy for the strength of the coupling between the superconductors forming the Josephson junction.

The pattern observed is, however, only qualitatively similar to conventional junctions. The most prevalent deviation is the hexagonal shape in the Shapiro steps, most

prominently seen in the 4 (Fig. 3d) and 4.5 GHz (Fig. 3e) data. Further, there is also an unconventional power dependence of the peak width, essential in extracting the peak height from measurements of the differential resistance  $r$ . Unlike conventional junctions where the peak height is uniform, here we observe regions where the peak height almost disappears, seen most clearly in Fig. 3b,c (indicated by the white arrow). This makes an exact extraction of the peak height difficult. The peak heights do, however, increase with increasing frequency as expected for Josephson junctions. Finally, the transition from the superconducting state at  $P = 0$  proceeds in an unexpected manner, as seen in Sample II. Rather than peeling off from the superconducting to normal state transition, the inner features originate from a point at  $I_{DC} = 0$ . For comparison, plots of the Shapiro step diagram for conventional Josephson junctions at low and high values of  $f_c$  are given in the supplementary information [23].

Perhaps the most striking distinction between the inner and outer features is their respective dependence on an applied magnetic field. Contrary to the conventional Josephson effect, the inner features demonstrate an insensitivity to an applied magnetic field. By contrast, the outer features exhibit a conventional magnetic diffraction pattern expected for long Josephson junctions. This contrasting behavior in magnetic field is displayed in Fig. 4a,b for Samples I and II. The plots are taken under RF radiation of  $5\text{ GHz}$  (Fig. 4a) and  $7\text{ GHz}$  (Fig. 4b). The outer features associated with the PSL show a diffraction pattern expected for Josephson junctions (Fig. 4a,b). The inner features however, display an entirely different behavior. Clear field-independent peaks in  $r$  (indicated by black arrows) that correspond to the RF generated peaks are observed over the range of magnetic field of one quantum of flux, measured by the first node in the

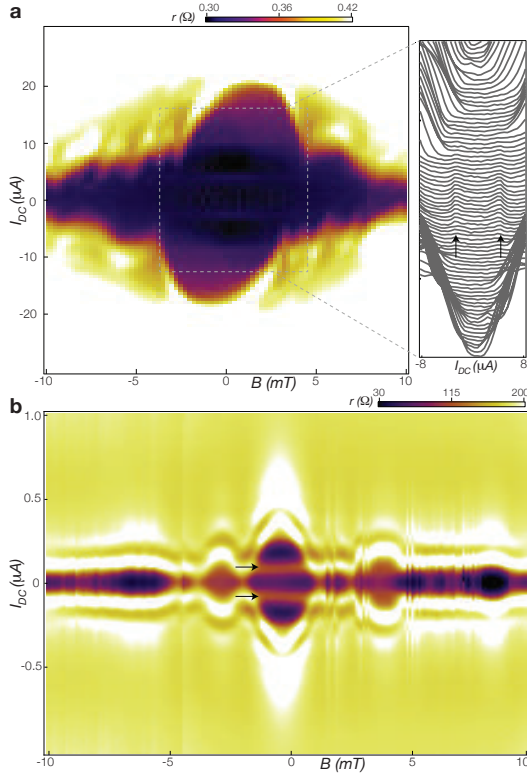


FIG. 4: **a,b.** Magnetic field dependence of the Shapiro steps for Samples I ( $f = 5\text{ GHz}$ ,  $P = -17.5\text{ dBm}$ ) and II ( $f = 7\text{ GHz}$ ,  $P = -10\text{ dBm}$ ). In addition to the Fraunhofer-like pattern observed in the outer features, a magnetic field independent peaks in  $r$  are observed for the inner features in each sample for values of applied flux less than  $\Phi_0$  (indicated in each figure by black arrows). The peaks in **a** are faint, so cuts of constant  $B$  the figure are shown on the right.

magnetic diffraction pattern of the outer features. Beyond this field, it is difficult to differentiate the inner and outer features.

We now discuss possible origins for this new type of Josephson effect observed. Three possible candidates are identified for the origin of this effect: an additional PSL created by the RF radiation, Shapiro steps originating from the CDW, and an interband phase slip. We rule out the first two possibilities. An additional PSL is indeed possible, however, the magnetic field dependence is absent, unlike the outer features which shows an expected magnetic diffraction pattern. The similarity between the equations governing the CDW and Josephson junction dynamics allows for Shapiro steps to be observed in materials like  $\text{NbSe}_3$  [24]. The primary difference is that the dynamical equation for CDW is one for the voltage produced by the sliding mode of the CDW. Hence, although the pattern is also described by a Bessel function dependence on RF power, the differential resistance is locally a maximum in the regions of the Shapiro steps, separated by regions of lower resistance [23]. Hence the pattern in  $r$  observed is not matched by the expectations

for a CDW. We also note that the AC-dependent voltage step height is of order  $10\text{ mV/GHz}$  [24], roughly three orders of magnitude higher than expected for Josephson junctions and four orders of magnitude greater than the typical peak height is observed in Sample I and II.

Multiband superconductivity allows for an additional degree of freedom to be introduced to the superconducting state. If the coupling between bands is weak compared to the intraband pairing strength, the Ginzburg-Landau free energy has an added term  $2J|\Delta_1||\Delta_2|\cos(\phi_1-\phi_2)$ , where the superconducting order parameter on each band is  $|\Delta_{i=1,2}|e^{i\phi_{i=1,2}}$  and  $J$  is the strength of the interband coupling. Important in this description is that the interband coupling mimics the Josephson relation. Theoretical expectations are that superconductors like  $\text{NbSe}_2$  [12] should be described by this equation, and indirect evidence on this effect in  $\text{NbSe}_2$  has been claimed [4–6]. It has also been observed that the amplitude of the order parameter is layer-number dependent [6], which may explain why the  $B$ -independent Josephson effect is only observed in our thinnest samples.

The ground state is obtained by the minimization which produces a phase  $\phi$  of either  $0$  or  $\pi$  depending on the sign of  $J$ . However, localized excitations which produce kinks in the phase are possible because of the degenerate minimum provided by the  $\cos(\phi)$  dependence of the interband coupling. Such an excitation – a soliton – is similar to soliton of flux produced in long Josephson junctions [10]. However, the key difference is its response to electromagnetic fields: the application of a magnetic field induces a phase shift that is identical in each band. Hence, such a slip in the phase does not respond to electromagnetic fields [10, 25]. Despite this insensitivity, manifestations on transport have been theoretically predicted in both system in both equilibrium [26] and out of equilibrium [27]; in equilibrium, experimental investigations of artificial two band superconductors have been performed [28]. We propose that this effect may be the origin of our observed phenomena and insights given by this experiment should help guide future theoretical and experimental developments.

*Acknowledgements:* We thank Sergiy Krylyuk and Albert Davydov for technical discussion including materials preparation. This work was sponsored by the grants National Science Foundation Physics Frontier Center at the Joint Quantum Institute (PHY-1430094).

---

- [1] A. V. Koloboc and J. Tominaga, “Two-Dimensional Transition-Metal Dichalcogenides” (Springer Publishing, United States, 2016).
- [2] M. M. Ugeda *et al.*, Characterization of collective ground states in single-layer  $\text{NbSe}_2$ . *Nature Phys.* **12**, 92 (2016).
- [3] Chao-Sheng Lian, Chen Si, and Wenhui Duan, Unveiling Charge-Density Wave, Superconductivity, and Their

Competitive Nature in Two-Dimensional NbSe<sub>2</sub>. *Nano Lett.* **18**, 2924 (2018).

[4] T. Yokoya, T. Kiss, A. Chainani, S. Shin, M. Nohara, and H. Takagi, Fermi Surface Sheet-Dependent Superconductivity in 2H-NbSe<sub>2</sub>, *Science* **294**, 2518 (2001).

[5] E. Boaknin, *et al.*, Heat Conduction in the Vortex State of NbSe<sub>2</sub>: Evidence for Multiband Superconductivity, *Phys. Rev. Lett.* **90**, 117003 (2003).

[6] T. Dvir, *et al.*, Spectroscopy of bulk and few-layer superconducting NbSe<sub>2</sub> with van der Waals tunnel junctions. *Nature Comm.* **9**, 598 (2018).

[7] X. Xi, *et al.*, Ising pairing in superconducting NbSe<sub>2</sub> atomic layers. *Nature Phys.* **12**, 139 (2016).

[8] U. Yaron, *et al.*, Neutron Diffraction Studies of Flowing and Pinned Magnetic Flux Lattices in 2H-NbSe<sub>2</sub>, *Phys. Rev. Lett.* **73**, 2748 (1994).

[9] J. Okamoto, C. J. Arguello, E. P. Rosenthal, A. N. Pasupathy, and A. J. Millis, Experimental Evidence for a Bragg Glass Density Wave Phase in a Transition-Metal Dichalcogenide, *Phys. Rev. Lett.* **114**, 026802 (2015).

[10] Y. Tanaka, Soliton in Two-Band Superconductor. *Phys. Rev. Lett.* **88**, 017002 (2002).

[11] Y. Tanaka, *et al.*, Topological structure of the inter-band phase difference soliton in two-band superconductivity. *Physica C* **470**, 1010 (2010).

[12] Y. Tanaka, Multicomponent superconductivity based on multiband superconductors. *Supercond. Sci. techno.* **28**, 034002 (2010).

[13] Y. Tanaka, Superconducting frustration bit. *Physica C* **505**, 55 (2014).

[14] Y. Tanaka, H. Yamamoria, T. Yanagisawa, T. Nishiob, S. Arisawac, Experimental formation of a fractional vortex in a superconducting bi-layer. *Physica C* **548**, 44 (2018).

[15] A. Maldonado, S. Vieira, and H. Suderow, “Supercurrent on a vortex core in 2H-NbSe<sub>2</sub>: Current-driven scanning tunneling spectroscopy measurements”, *Phys. Rev. B*, **88**, 064518 (2013).

[16] M. Tinkham, “Introduction to Superconductivity”, Chapter 11 (Dover Publishing, United States 1996).

[17] A. G. Sivakov, *et al.*, Josephson Behavior of Phase-Slip Lines in Wide Superconducting Strips. *Phys. Rev. Lett.* **91**, 267001 (2003).

[18] Nicola Paradiso, Anh-Tuan Nguyen, Karl Enzo Kloss, and Christoph Strunk, Phase slip lines in superconducting few-layer NbSe<sub>2</sub> crystals. arXiv:1811.06207v1 (2018).

[19] A. Barone, G. Paternò, *Physics and Applications of the Josephson Effect*. (Wiley-Interscience Publications, Canada 1982).

[20] X. Xi, *et al.*, Strongly enhanced charge-density-wave order in monolayer NbSe<sub>2</sub>. *Nature Nano.* **10**, 765 (2015).

[21] M. I. Visscher and B. Rejaei, Josephson Current through Charge Density Waves. *Phys. Rev. Lett.* **79**, 4461 (1997).

[22] M. S. El-Bana, *et al.*, Superconductivity in two-dimensional NbSe<sub>2</sub> field effect transistors. *Supercond. Sci. techno.* **26**, 125020 (2013).

[23] Supplementary information will be given at the time of publication.

[24] A. Zettl and G. Grüner, Phase coherence in the current-carrying charge-density-wave state: ac-dc coupling experiments in NbSe<sub>3</sub>. *Phys. Rev. B* **29**, 755 (2003).

[25] David Pekker and C.M. Varma, Amplitude/Higgs Modes in Condensed Matter Physics. *Annu. Rev. Condens. Matter Phys.* **6**, 269 (2015).

[26] A. Gurevich and V. M. Vinokur, Phase Textures Induced by dc-Current Pair Breaking in Weakly Coupled Multilayer Structures and Two-Gap Superconductors. *Phys. Rev. Lett.* **97**, 137003 (2006).

[27] A. Gurevich and V. M. Vinokur, Interband Phase Modes and Nonequilibrium Soliton Structures in Two-Gap Superconductors. *Phys. Rev. Lett.* **90**, 047004 (2003).

[28] Hendrik Bluhm, Nicholas C. Koshnick, Martin E. Huber, and Kathryn A. Moler, Magnetic response of mesoscopic superconducting rings with two order parameters. *Phys. Rev. Lett.* **97**, 237002 (2006).